

Development of a novel AIE active Piperazine appended Chemosensor for solvent-regulated selective detection of IIB elements [Zn(II), Cd(II), Hg(II)], Cl⁻ and picric acid via varying emission colors to distinguish one another: environmental and biological applications

Manik Das ^a, Pranabendu Das^a, Shubham Ray^a, Arijit Bag^b, Soumik Laha ^c, Indranil Choudhuri^d, Nandan Bhattacharya^d, Bidhan Chandra Samanta^e, Tithi Maity^a

^aDepartment of Chemistry, Prabhat Kumar College, Contai, Purba Medinipur, West Bengal, 721404, India

^bIndian Institute of Chemical Biology, Jadavpur, Kolkata, West Bengal, India.

^cSchool of Natural and Applied Sciences, Maulana Abul Kalam Azad University of Technology, West Bengal, India

^dDepartment of Biotechnology, Panskura Banamali College, Panskura West Bengal, India.

^eDepartment of Chemistry, Mugberia Gangadhar Mahavidyalaya, Purba Medinipur, India

Email: titlipkc2008@gmail.com

Sl. No.	Index	Page Number
1.	Uv absorption spectra of HL (Fig. S1)	S4
2.	FTIR Spectrum of HL (Fig. S2)	S4
3.	Mass Spectrum of HL (Fig. S3)	S5
4.	¹ H NMR spectrum of HL (Fig. S4)	S5
5.	¹³ C NMR spectrum of HL (Fig. S5)	S6
6.	Fluorescence Emission Spectra of HL (10 μM) at λ _{max} = 520 nm in EtOH / H ₂ O buffer system (pH = 7.4) by varying water volume fraction up to 99% (Fig. S6)	S6
7.	Uv absorption spectra of HL (10 μM) in EtOH / H ₂ O buffer system (pH = 7.4) by varying water volume fraction (Fig. S7)	S7
8.	DLS experiment of HL with the variation of volume of water fraction (Fig. S8)	S7

	S8)	
9.	SEM Images of HL at scale bar a) 1 μM and b) 200 μM (b) (Fig. S9)	S8
10.	Fluorescence intensity change of HL after the addition of (a) chloride/perchlorate salt of cations (2.0 eq) (b) TBA salt of anions (2.0 eq) in EtOH/H ₂ O HEPES buffer (9:1) medium (pH 7.4) (c) chloride salt of cations (2.0 eq) in AIEE solvent (EtOH/H ₂ O HEPES buffer (1:9 v/v) medium (pH 7.4) (Fig. S10)	S8
11.	Uv Spectroscopic titration response of HL towards Zn(II), Cd(II), Hg(II) and Cl ⁻	S9
12.	Uv absorption titration graph of HL (10 μM) upon addition of (a) Zn(II) (0 – 20 μM) in EtOH/H ₂ O HEPES buffer (9:1) medium (pH 7.4) (b) Cd(II) (0 – 20 μM) In EtOH/H ₂ O HEPES buffer (1:9 v/v) medium (pH 7.4) (c) Hg(II) (0 – 20 μM) In EtOH/H ₂ O HEPES buffer (1:9 v/v) medium (pH 7.4) (d) Cl ⁻ (0 – 20 μM) in EtOH/H ₂ O HEPES buffer (9:1) medium (pH = 7.4) (Fig. S11)	S9
13.	Binding Constant determination plot during sensing of (a) Zn ²⁺ (b) Cd ²⁺ (c) Hg ²⁺ , and (d) Cl ⁻ by chemosensor HL (Fig. S12)	S10
14.	Change of fluorescence emission intensity of HL as a function of (a) Zn ²⁺ , (b) Cd ²⁺ , and (c) Cl ⁻ ion concentration for Limit of Detection (LOD) calculation semi aqueous and aqueous medium (Fig. S13)	S11
15.	a) During recognition of Zn(II) in ethanol-water medium b) Cd(II) in HEPES buffer medium c) Cl ⁻ in the ethanol-water medium by HL , the Binding constant measurement by utilizing probe-analyte fluorescence enhancement titration pictograph. (Fig. S14)	S11
16.	(a) The variation of absorbance of HL ($3 \times 10^{-5} \text{ M}^{-1}$) as a function of time in ethanol: H ₂ O (9:1) HEPES buffer medium b) In different pH the variation of the fluorescence intensity changes of bare HL ($3 \times 10^{-5} \text{ M}^{-1}$) a) at 325 nm in the absence and presence (four equivalent) of Zn(II) in ethanol-water HEPES buffer medium whereas at 358 nm in the presence and absence of Hg(II)/Hg(II) in the near aqueous medium. (Fig. S15)	S12
17.	a) HL -Zn(II) adduct fluorescence intensity alteration at 325 nm after alternative addition of EDTA and Zn(II) in semi-aqueous medium displaying the existence of reversibility during sensing phenomenon. (Fig. S16)	S12

18.	Fluorescence emission change of (a) HL-Zn(II) adduct in presence of four equivalents of various competitive cations in semi-aqueous medium (b) HL-Cd(II) in presence of four equivalents of various competitive cations in aqueous medium (c) HL-Hg(II) adduct in presence of four equivalents of various competitive cations in aqueous medium and (d) HL-Cl⁻ adduct in presence of several anions (Fig. S17).	S13
19.	Selective sensing of Zn(II)/Cl ⁻ /Cd(II) in simultaneous presence Zn(II)/Cl ⁻ /Cd(II)/Hg(II) semi-aqueous and near aqueous medium(Fig. S18)	S13
20.	Fluorescence response of HL towards different NACs (Fig. S19)	S14
21.	Binding Constant determination plot of the probe HL (20 μM) after the addition of PA (0 – 30μM) (b) change of fluorescence intensity of HL as a function of the concentration of PA plot to determine LOD during the reorganization of PA (c) Quenching Constant determination Plot of HL after addition of PA (Fig. S20).	S14
22.	Jobs plot of 1:1 complex formation during sensing of a) Zn(II) b) Cd(II) c)(II) (d) Cl ⁻ and (e) PA by chemosensor HL (Fig. S21)	S15
23.	Mass spectra of HL-Zn complex (Fig. S22)	S16
24.	Mass spectra of HL-Cd complex (Fig. S23)	S16
25.	Mass spectra of HL-Hg complex (Fig. S24)	S17
26.	Combined FTIR Spectra of a) HL , HL-Zn(II) , HL-Cd(II) , HL-Hg(II) Complexes b) HL , HL-TBA-Cl (Fig. S25)	S17
27.	DFT optimized structure of (a) HL , (b) HL-Zn Complex, (c) HL-Cd Complex,(d) HL-Hg Complex, (e) HL-Cl Complex, and (f) HL-PA Complex.(Fig. 26)	S18
28.	Quantification of Cd(II) in a)tap water b) distilled water c) industrial area river water and Hg(II) in a) tap water b) Industrial water c) Industrial river water (Fig. S27)	S19
29.	Dose-dependent suppression of cell viability of HL on HeLa cell line (24 hrs) (Fig. S28)	S19
30.	Literature report of picric acid sensing by organic probe (Table S1)	S20
31.	Results of Hg ²⁺ determination by the sensor HL in three real water samples (Table S2)	S21

32.	Results of Cd ²⁺ determination by the sensor HL in three real water samples (Table S3)	S22
-----	--	-----

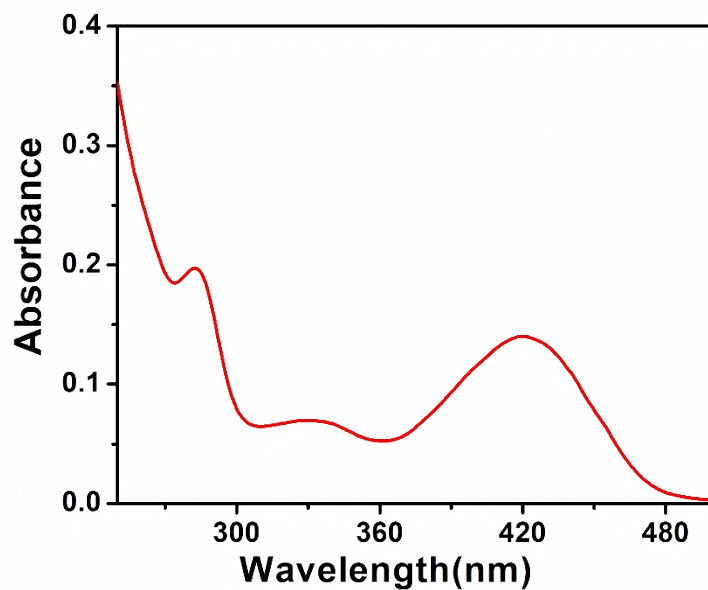


Fig. S1: UV spectrum of HL

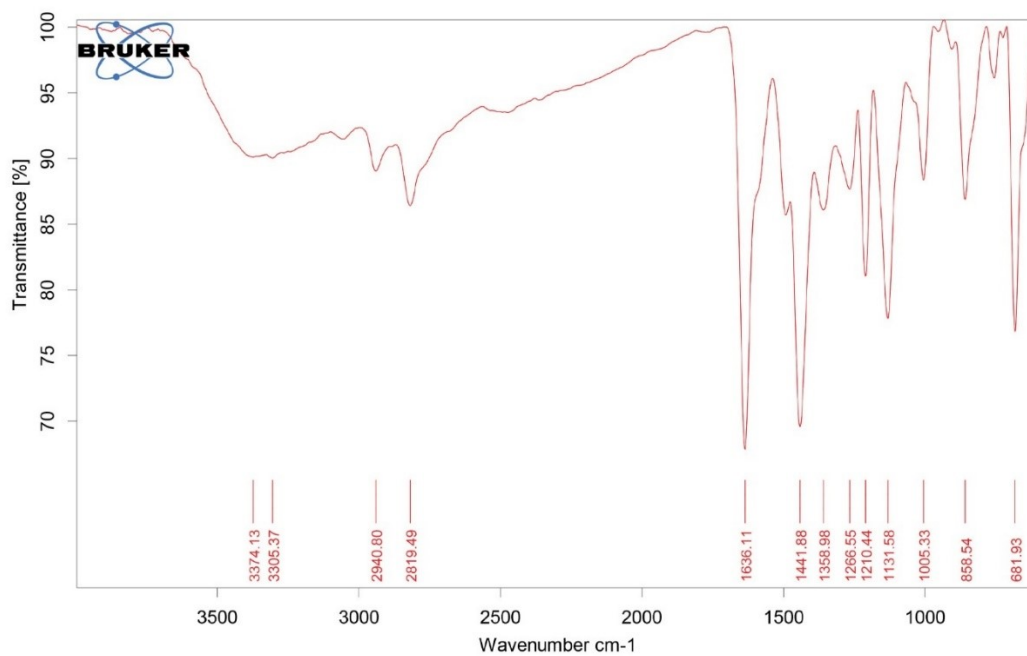


Fig. S2: FTIR spectrum of HL

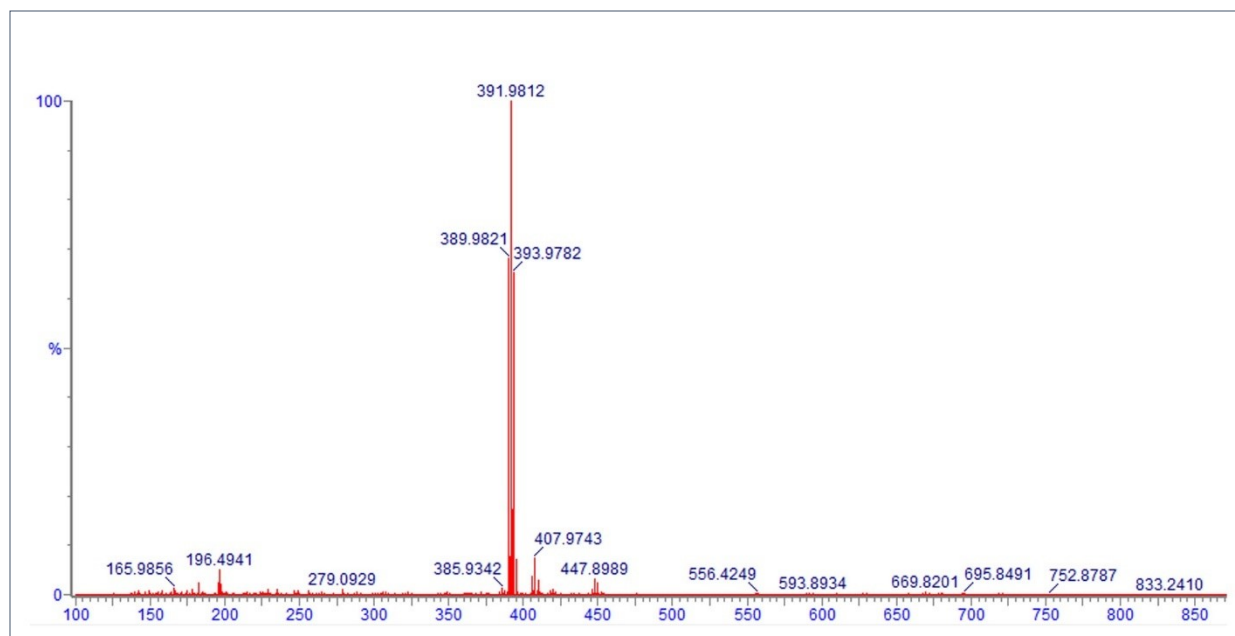


Fig. S3: Mass Spectrum of **HL**

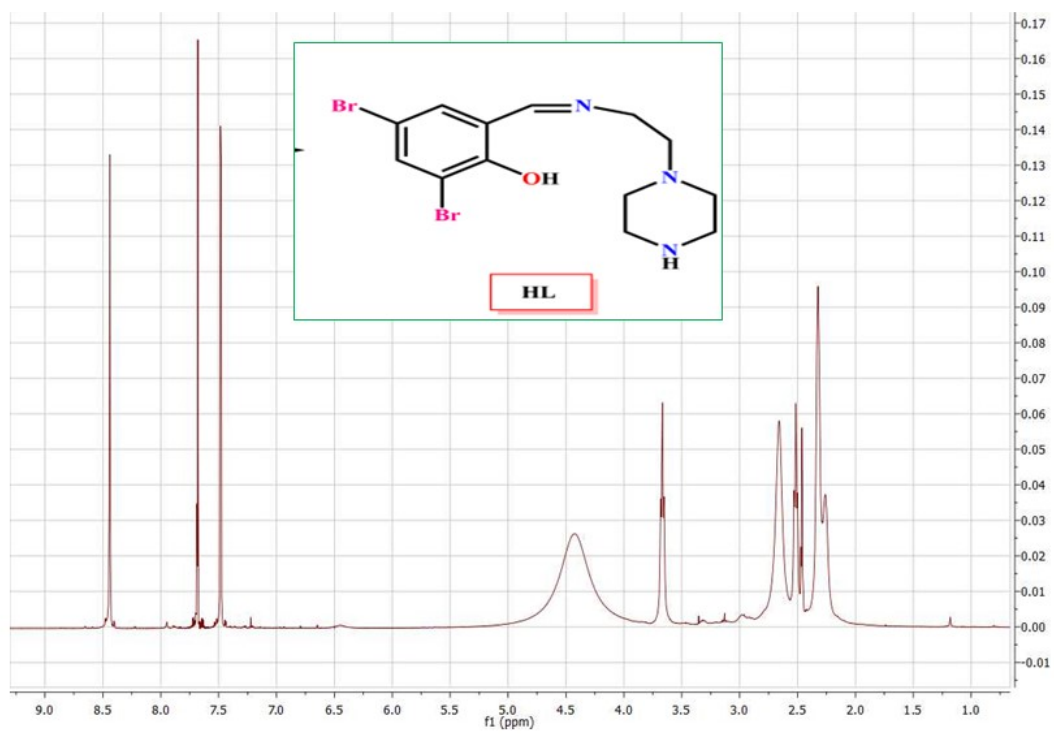


Fig. S4: ¹H NMR Spectrum of **HL**

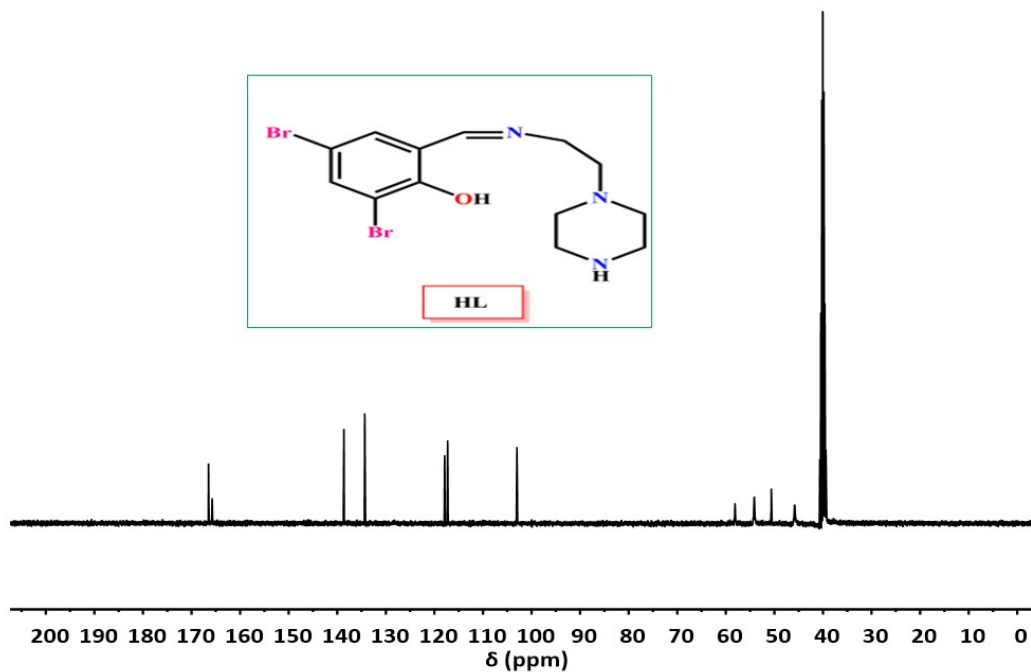


Fig. S5: ^{13}C NMR Spectrum of **HL**

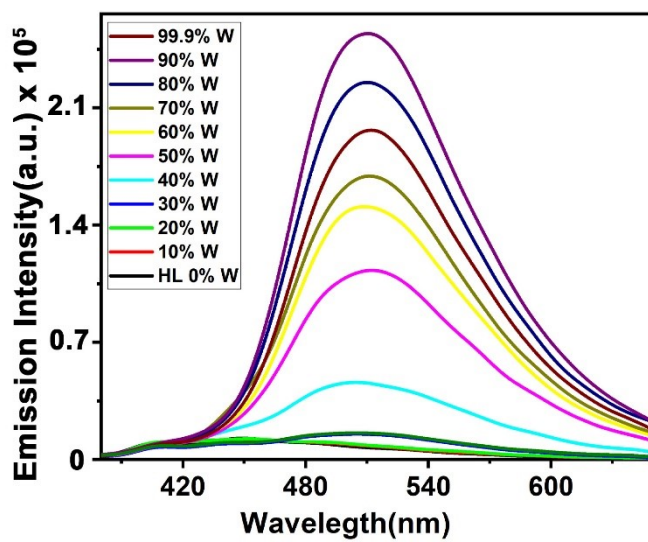


Fig. S6: Fluorescence emission Spectra of **HL** ($10\ \mu\text{M}$) at $\lambda_{\text{max}} = 520\ \text{nm}$ in EtOH / H_2O buffer system ($\text{pH} = 7.4$) by varying water volume fraction up to 99%

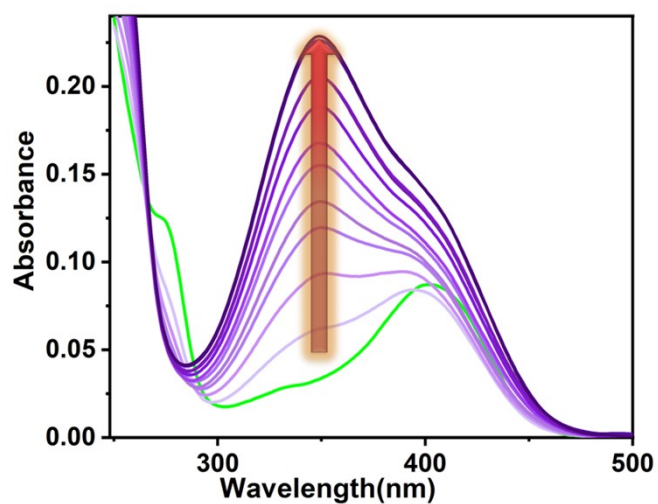


Fig. S7: UV absorption spectra of **HL** (10 μM) in EtOH / H₂O buffer system (pH = 7.4) by varying water volume fraction

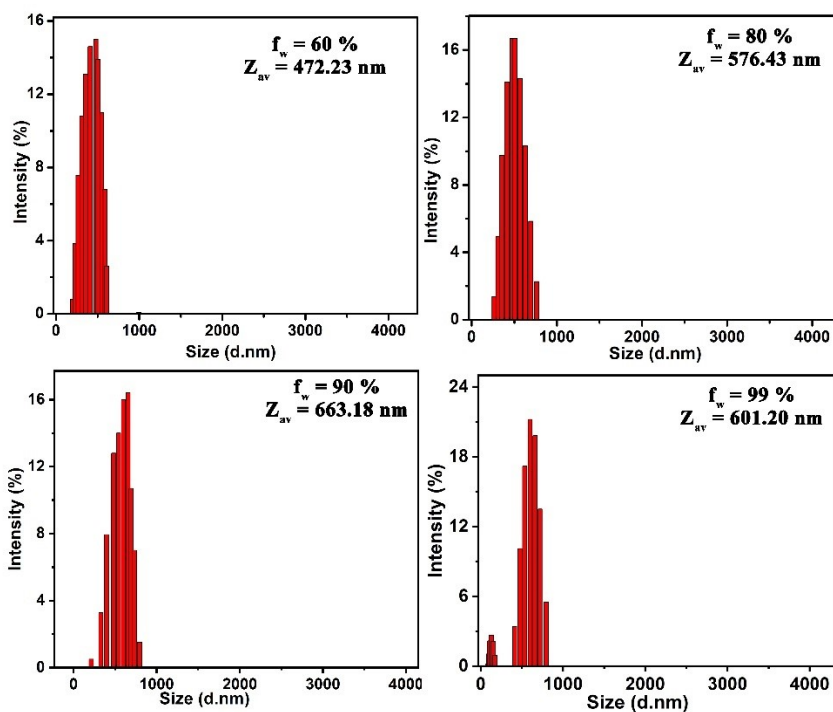


Fig. S8: DLS experiment of **HL** with the variation of volume of water fraction

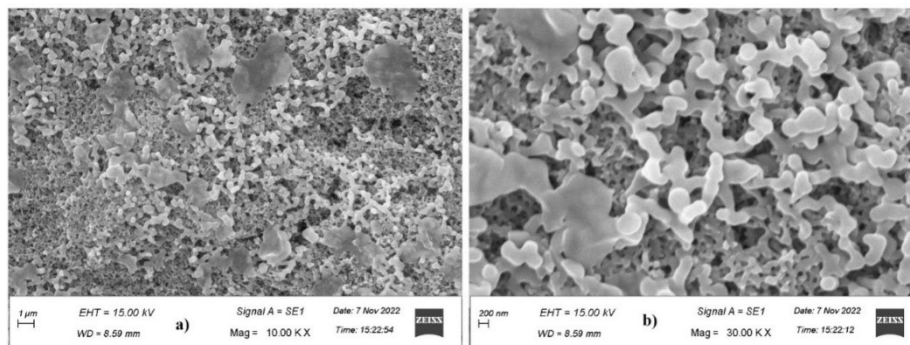


Fig. S9: SEM Images of HL at scale bar a) 1 μM and b) 200 μM (b)

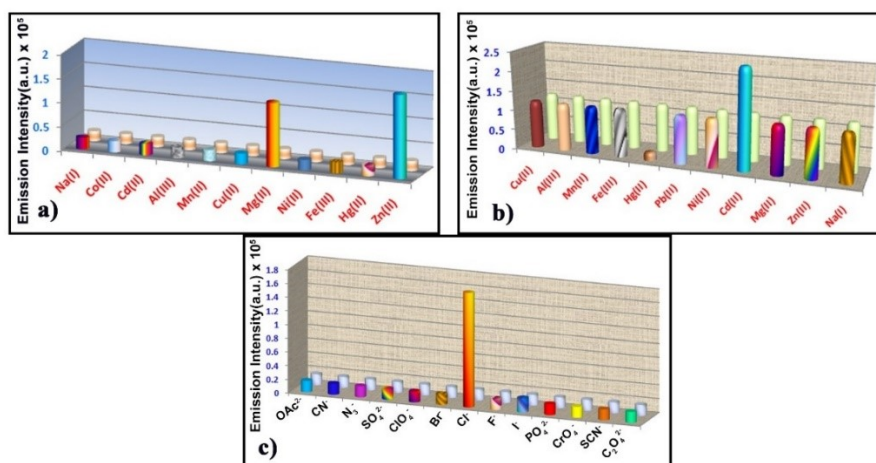


Fig. S10: Fluorescence intensity change of HL after the addition of (a) chloride/perchlorate salt of cations (2.0 eq) (b) TBA salt of anions (2.0 eq) in EtOH/H₂O HEPES buffer (9:1) medium (pH 7.4) (c) chloride salt of cations (2.0 eq) in AIEE solvent (EtOH/H₂O HEPES buffer (1:9 v/v) medium (pH 7.4)

***** **Cations:** Zinc (Zn²⁺), Copper (Cu²⁺), Magnesium (Mg²⁺), Aluminum (Al³⁺), Mercury (Hg²⁺), Iron (Fe³⁺), Nickel (Ni²⁺), Sodium (Na⁺), cobalt (Co²⁺), Cadmium (Cd²⁺), Lead (Pb²⁺) and Manganese (Mn²⁺).

Anions: Chloride (Cl⁻), Bromide (Br⁻), iodide (I⁻), Fluoride (F⁻), Azide (N₃⁻), Acetate (OAc⁻), Cyanide (CN⁻), Sulphate (SO₄²⁻), Oxalate (C₂O₄²⁻), Chromate (CrO₄²⁻), Phosphate (PO₄³⁻) and Perchlorate (ClO₄⁻)

Uv Spectroscopic titration response of HL towards Zn(II), Cd(II), Hg(II) and Cl⁻

To get an idea regarding the binding efficiency of **HL** towards the target analytes a detailed Uv absorption titration has been performed under identical experimental conditions. Primarily in a 9:1 ethanol-water medium the bare **HL** (10 μ M) displays three absorption bands at around 278 nm, 325 nm, and 425 nm and after the incremental addition of Zn(II) (0 – 20 μ M), the appearance of a new absorption band with red shift at around 390 nm is visualized along with a gradual decrease in the aforementioned absorption bands (**Fig. S11a**).

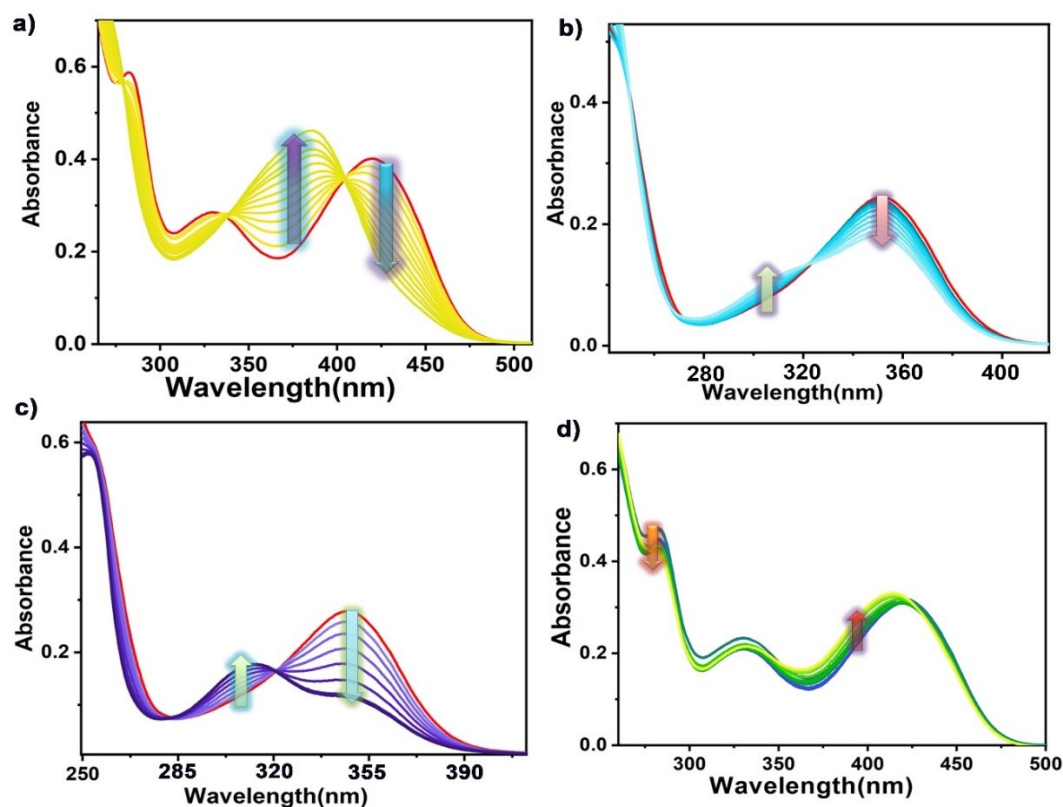


Fig. S11: Uv absorption titration graph of **HL** (10 μ M) upon addition of (a) Zn(II) (0 – 20 μ M) in EtOH/H₂O HEPES buffer (9:1) medium (pH 7.4) (b) Cd(II) (0 – 20 μ M) In EtOH/H₂O HEPES buffer (1:9 v/v) medium (pH 7.4) (c) Hg(II) (0 – 20 μ M) In EtOH/H₂O HEPES buffer (1:9 v/v) medium (pH 7.4) (d) Cl⁻ (0 – 20 μ M) in EtOH/H₂O HEPES buffer (9:1) medium (pH = 7.4)

At the same time in the same working medium, with systematic addition of Cl⁻ (0 – 20 μ M) to the probe **HL** the absorption bands at 325 nm and 278 nm gradually decrease while at 425 nm the hyperchromic shifting is observed (**Fig. S11d**). Two distinct isosbestic points at around 345 nm and 405 nm on the **HL**-Zn(II) titration plot and one distinct isosbestic point at 289 nm on

HL-Cl⁻ titration plot indicate the persistence of interchange between complexed and uncomplexed species. On the other hand, in 1:9 ethanol-water medium (AIE medium), after the introduction of Hg(II) (0 – 20 μM) and Cd(II) (0 – 20 μM), the absorption band of the probe at around 358 nm gradually decreases and at the same time, a new peak develops with slight blue shift on the titration plot at around 310 nm and 303 nm in the case of Cd(II) (**Fig. S11b**) and Hg(II) (**Fig. S11c**) respectively. In both systems, one distinct isosbestic point is seen at around 325 nm.

By applying the Benassi–Hildebrand equation, near inner fitting is done to measure the binding constants and these values are 5.45×10^6 (M⁻¹) for Zn(II), 3.87×10^6 (M⁻¹) for Cd(II), 3.38×10^6 (M⁻¹) for Hg(II), and 2.15×10^5 (M⁻¹) for Cl⁻ (**Fig. S12**). The high host-guest binding constant values accredit the chelation between the metal ions and the probe as the probe has N, N, and O coordination centers to bind with the metal center and The Cl⁻ ions is ascribed to the hydrogen bonding interaction between the Cl⁻ ion and the NH moiety in the **HL**.

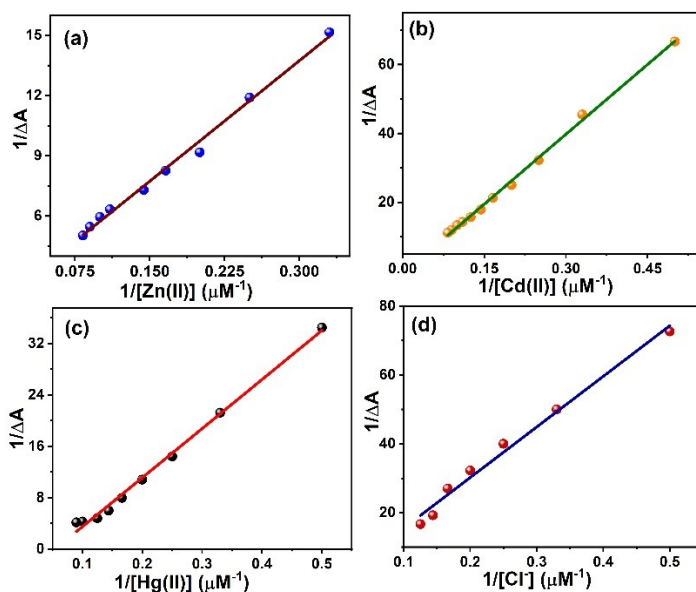


Fig. S12: Binding Constant determination plot during sensing of (a) Zn²⁺ (b) Cd²⁺ (c) Hg²⁺, and (d) Cl⁻ by chemosensor **HL**

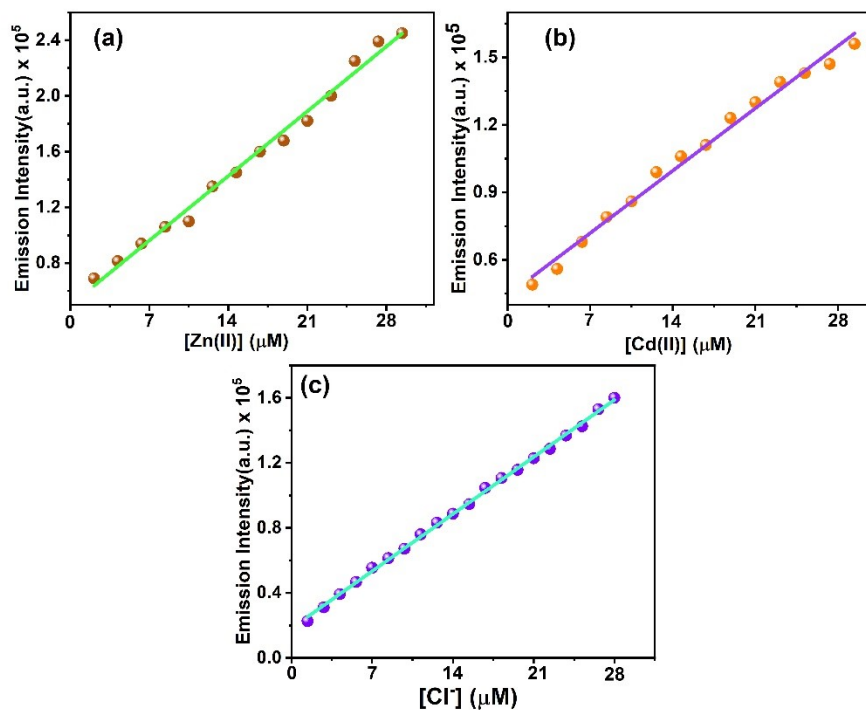


Fig. S13: Change of fluorescence emission intensity of **HL** as a function of (a) Zn²⁺, (b) Cd²⁺, and (c) Cl⁻ ion concentration for Limit of Detection (LOD) calculation semi aqueous and aqueous medium

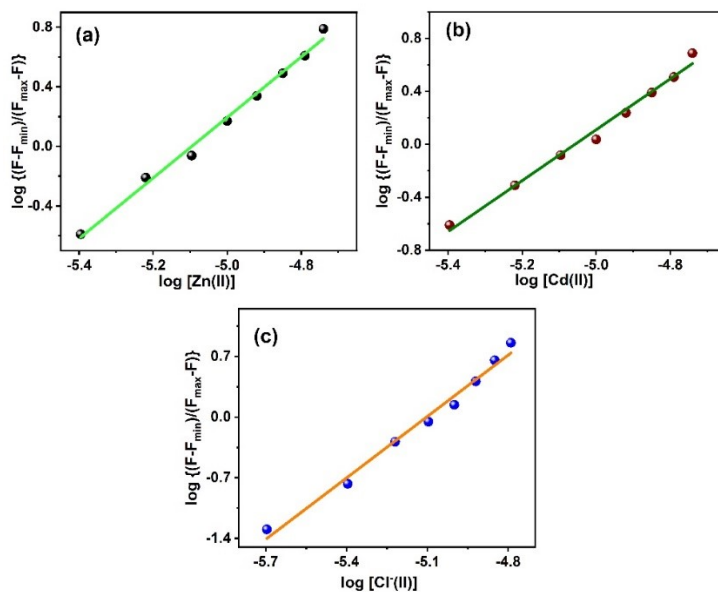


Fig. S14: a) During recognition of Zn(II) in ethanol-water medium b) Cd(II) in HEPES buffer medium c) Cl⁻ in the ethanol-water medium by **HL**, the Binding constant measurement by utilizing probe-analyte fluorescence enhancement titration pictograph

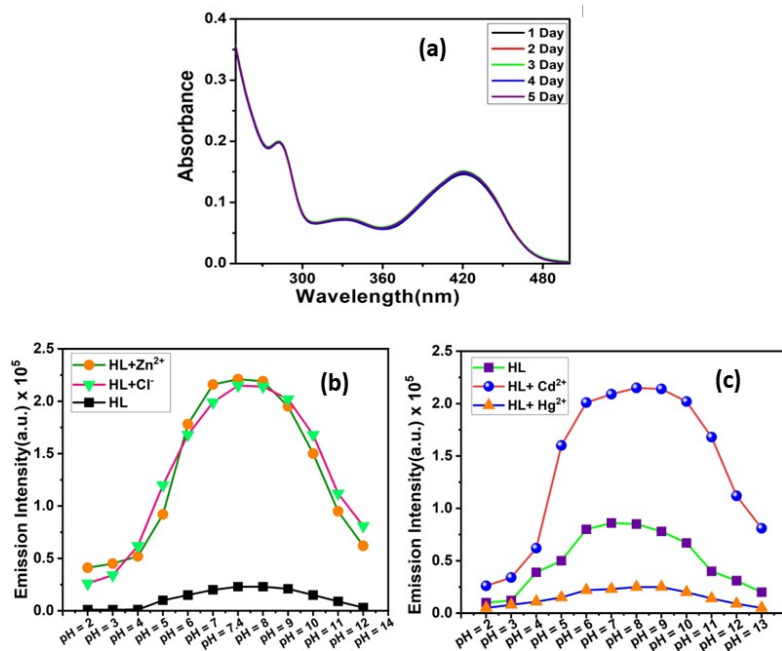


Fig. S15: (a) The variation of absorbance of **HL** ($3 \times 10^{-5} \text{ M}^{-1}$) as a function of time in ethanol: H₂O (9:1) HEPES buffer medium b) In different pH the variation of the fluorescence intensity changes of bare **HL** ($3 \times 10^{-5} \text{ M}^{-1}$) a) at 325 nm in the absence and presence (four equivalent) of Zn(II) and Cl⁻ in 9:1 ethanol-water HEPES buffer medium whereas c) 358 nm in the presence and absence of Cd(II)/Hg(II) in the near aqueous medium.

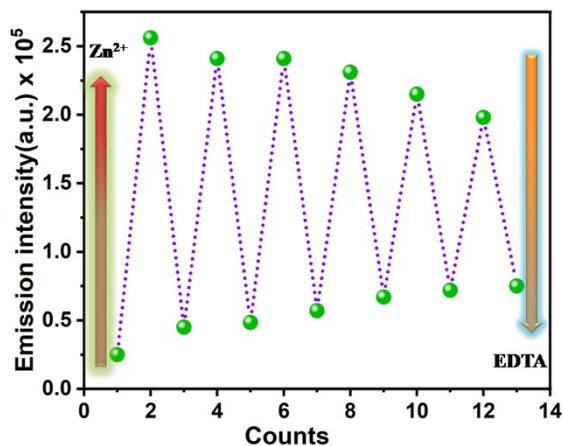


Fig. S16: a) **HL**-Zn(II) adduct fluorescence intensity alteration at 325 nm after alternative addition of EDTA and Zn(II) in semi-aqueous medium displaying the existence of reversibility during sensing phenomenon.

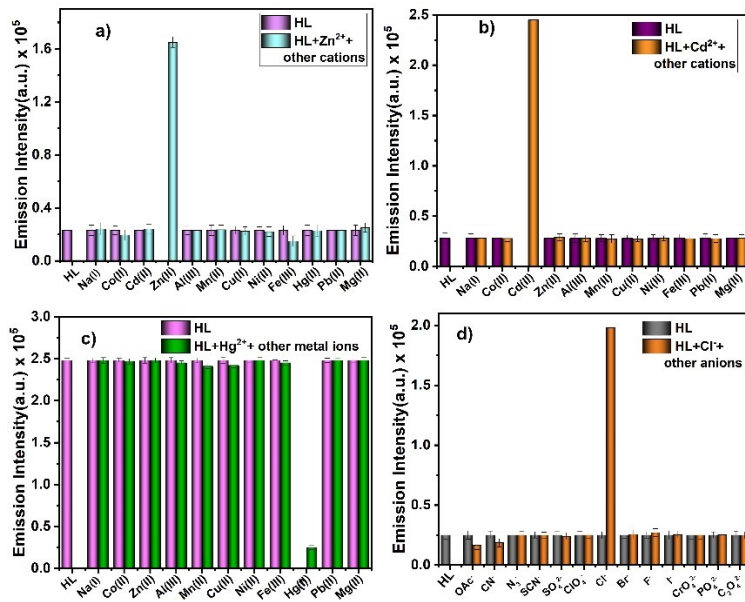


Fig. S17: Fluorescence emission change of (a) HL-Zn²⁺, (b) HL-Cd²⁺, (c) HL-Hg²⁺ adduct in presence of four equivalents of various competitive cations and (d) HL-Cl⁻ adduct in presence of several anions.

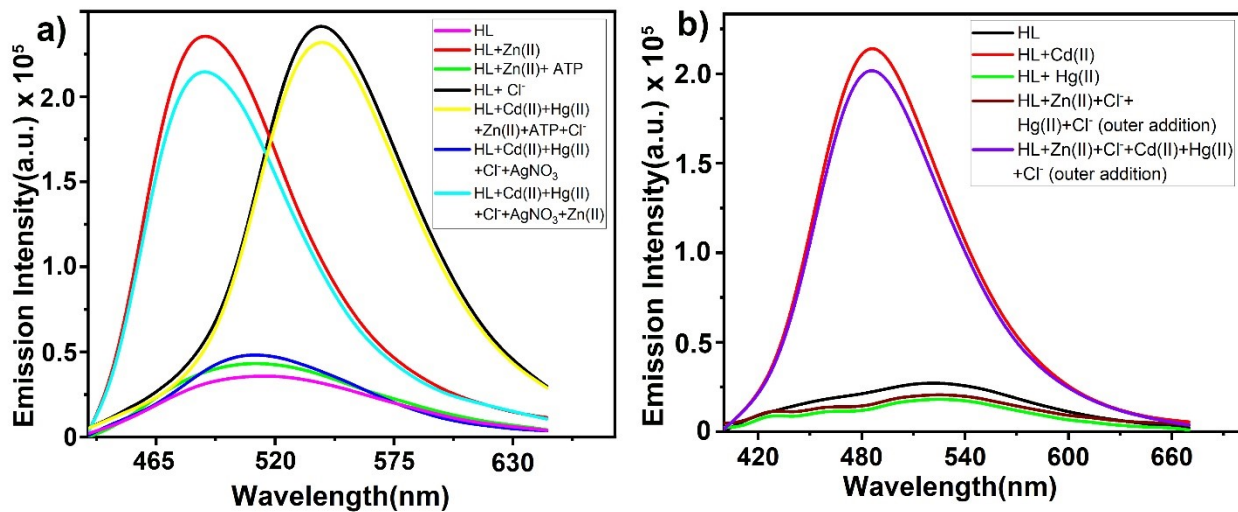


Fig. S18: Selective sensing of Zn(II)/Cl⁻/Cd(II) in simultaneous presence Zn(II)/Cl⁻/Cd(II)/Hg(II) semi-aqueous and near aqueous medium

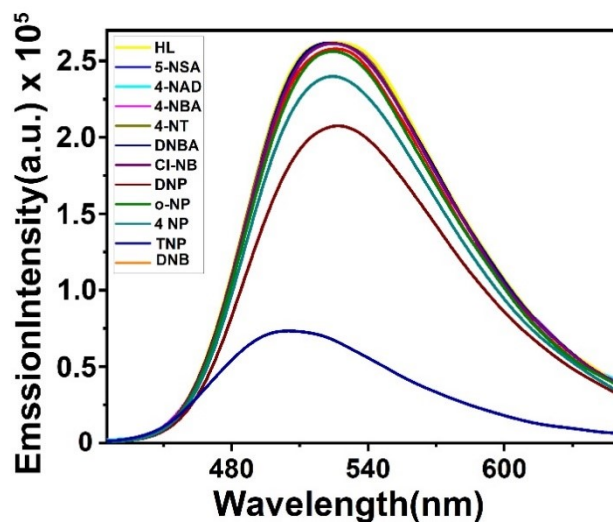


Fig. S19: Fluorescence response of **HL** towards different NACs

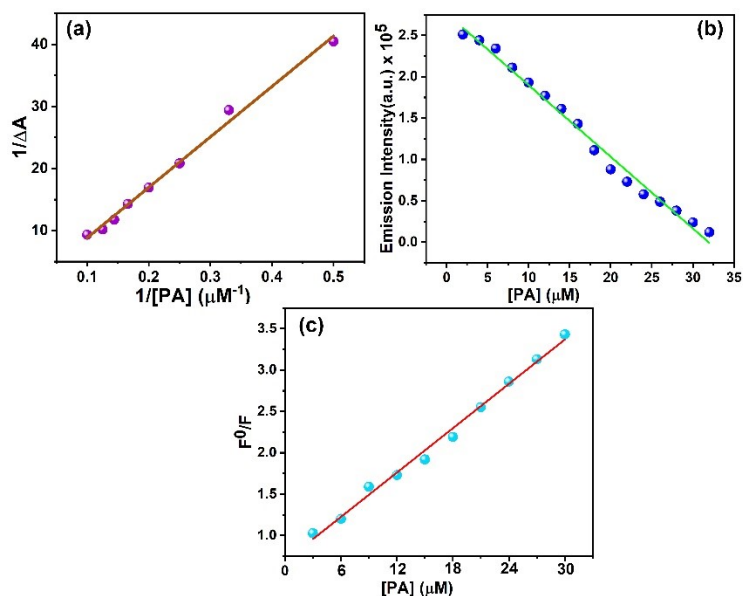


Fig. S20: Binding Constant determination plot of the probe **HL** (20 μM) after the addition of PA (0 – 30 μM) (b) change of fluorescence intensity of **HL** as a function of the concentration of PA plot to determine LOD during the reorganization of PA (c) Quenching Constant determination Plot of **HL** after addition of PA.

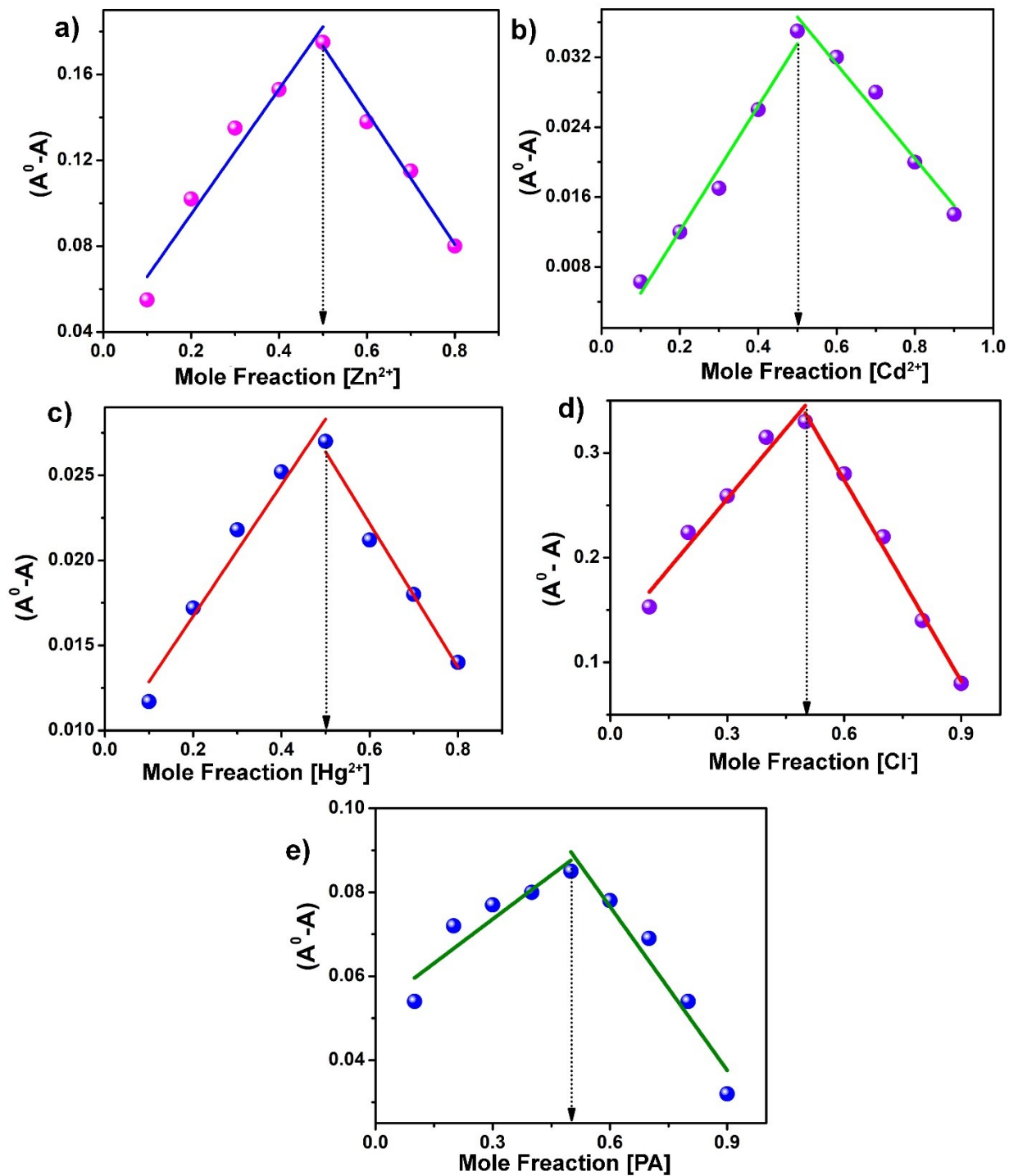


Fig. S21: Jobs plot of 1:1 complex formation during sensing of a) Zn²⁺ b) Cd²⁺ c) Hg²⁺ (d) Cl⁻ and (e) PA by chemosensor **HL**

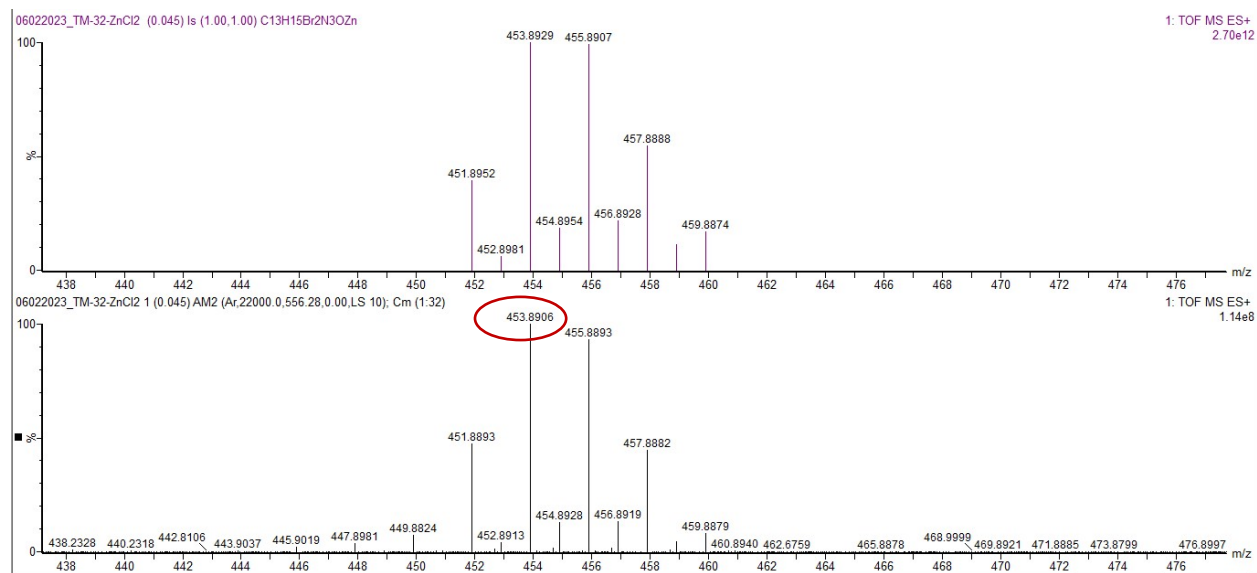


Fig. S22 Mass Spectra of HL- Zn complex

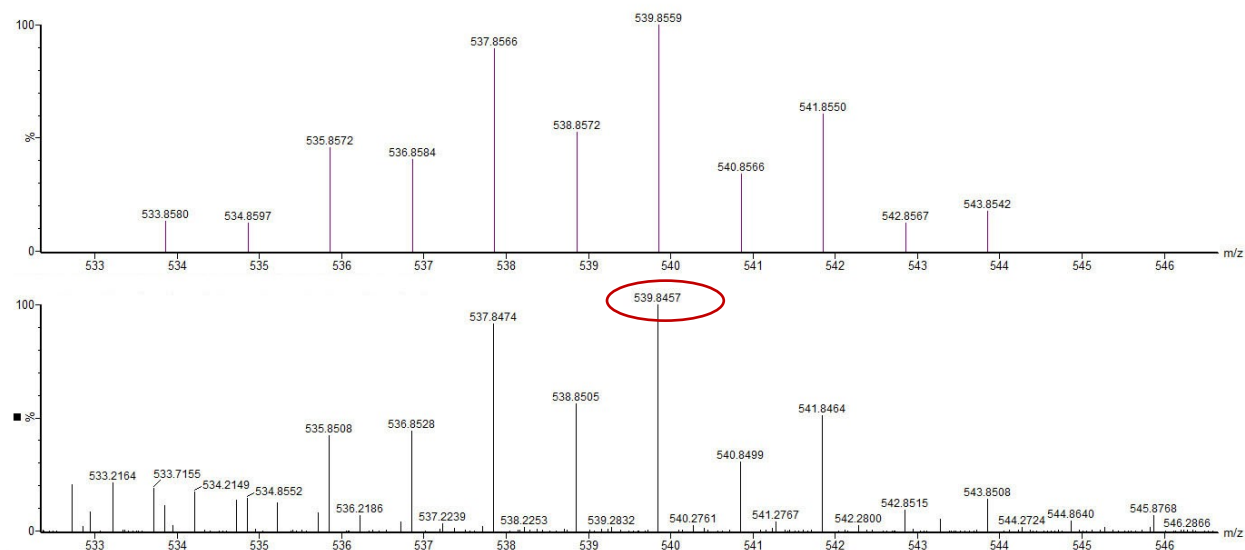


Fig. S23 Mass Spectra of HL- Cd complex (Isotopic Abundance)

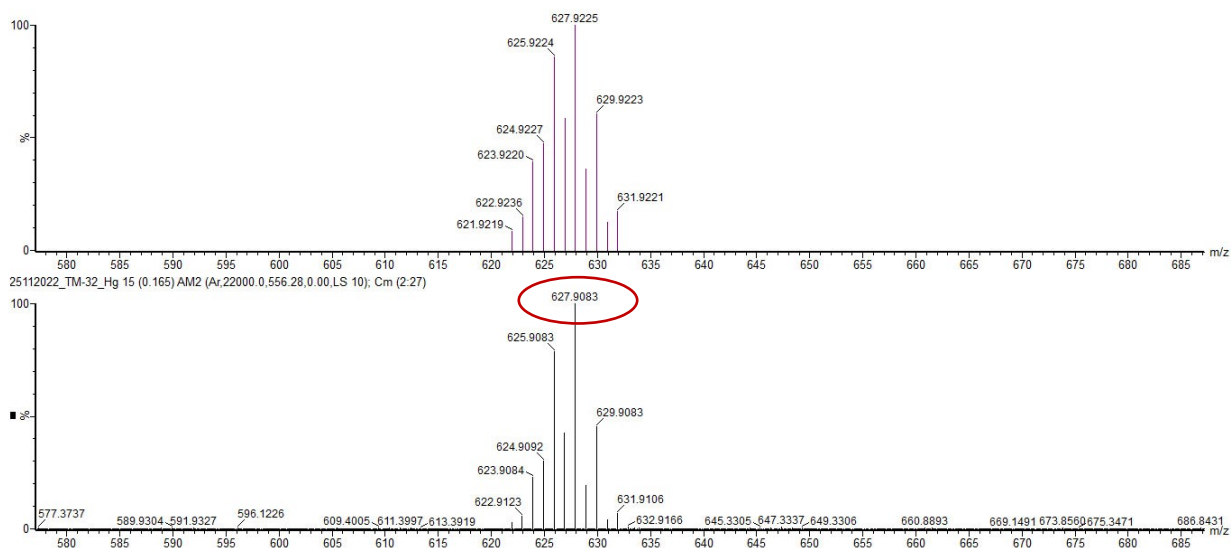


Fig. S24: Mass Spectra of HL-Hg Complex (Isotopic Abundance)

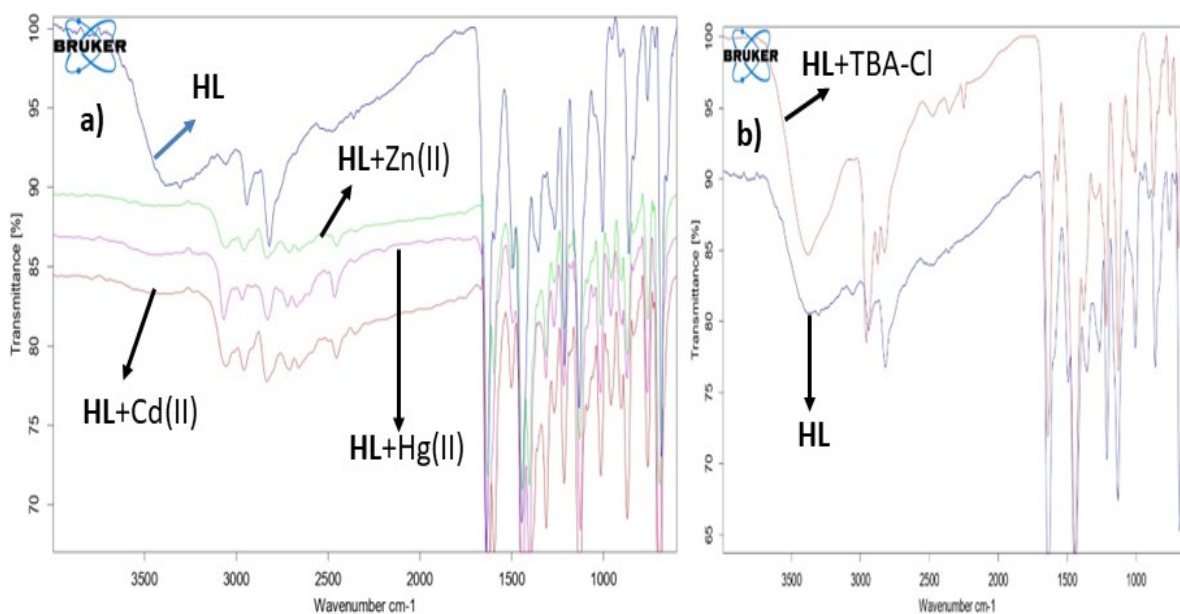


Fig. S25: Combined FTIR Spectra of a) HL, HL-Zn(II), HL-Cd(II), HL-Hg(II) Complexes
b) HL, HL-TBA-Cl

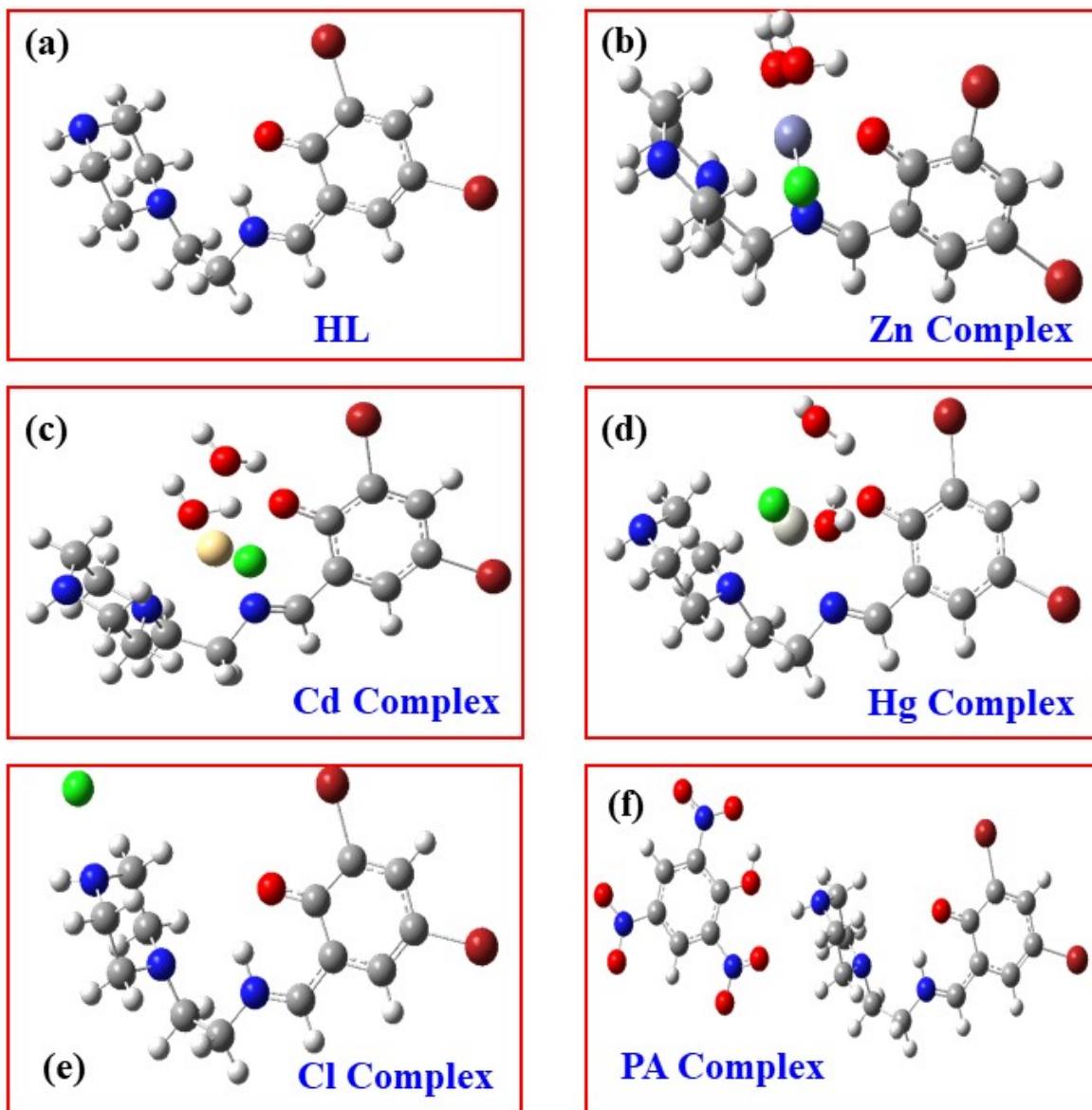


Fig. S26: DFT optimized structure of (a) HL, (b) HL-Zn Complex, (c) HL-Cd Complex, (d) HL-Hg Complex, (e) HL-Cl Complex, and (f) HL-PA Complex.

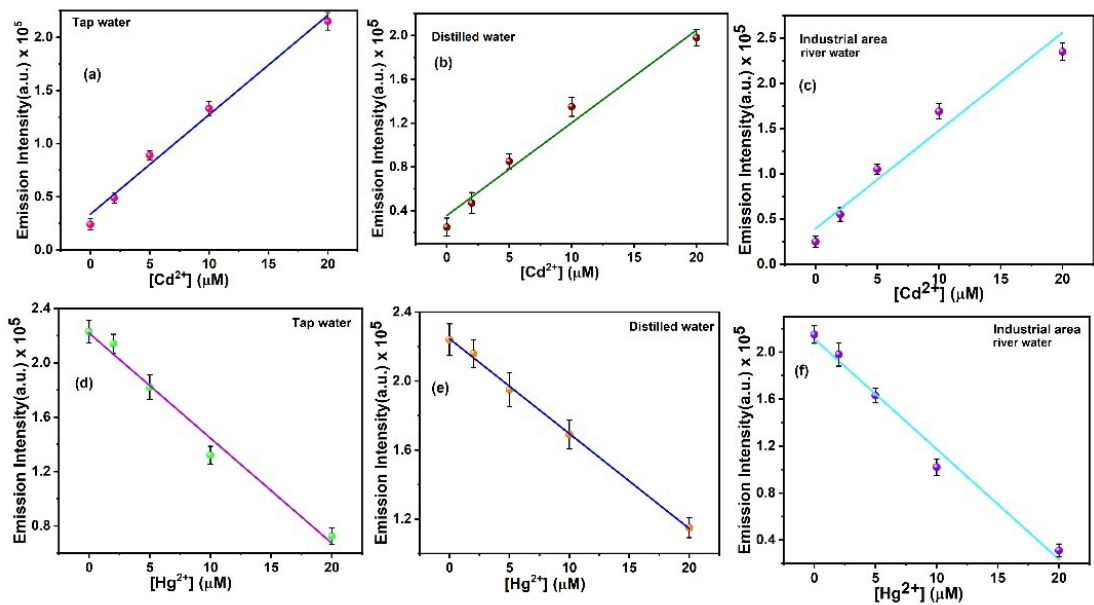


Fig. S27: Quantification of Cd(II) in a) tap water b) distilled water c) industrial area river water and Hg(II) in a) tap water b) Industrial water c) Industrial river water

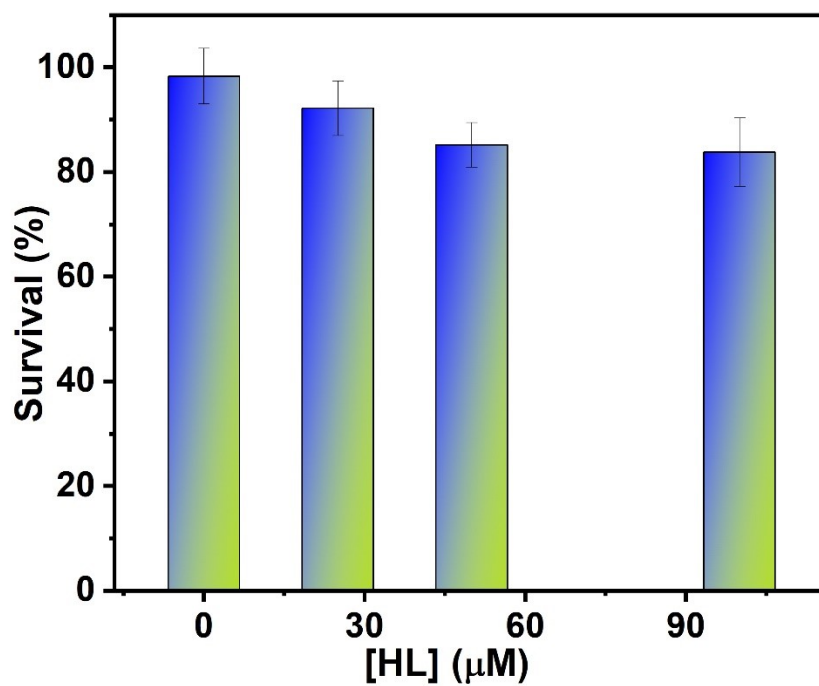


Fig S28: Dose-dependent suppression of cell viability of HL on HeLa cell line (24 hrs)

Table S1: Literature report of picric acid sensing by organic probe

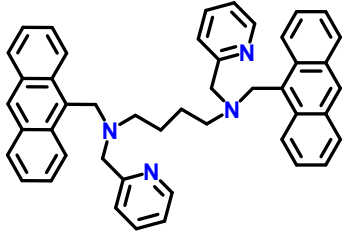
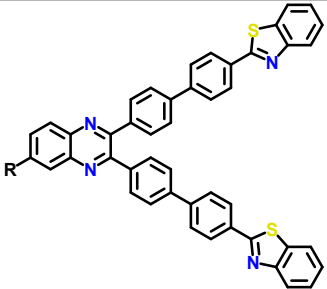
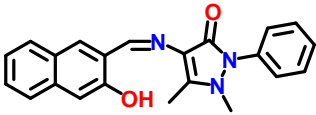
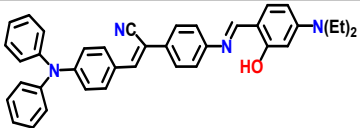
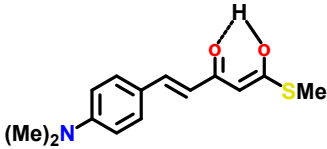
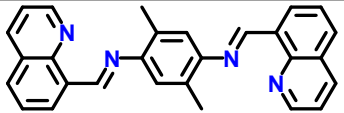
Entry	Probe	solvent	Sensing mode	LOD (10^{-6} M)	Reference
01		water	Turn OFF	0.6	1
02		THF	Turn OFF	1.32	2
03		MeOH:H ₂ O	Turn OFF	0.11	3
04		THF:H ₂ O	Turn OFF	1.26	4
05		THF:H ₂ O	Turn OFF	2.0	5
06		MeCN:H ₂ O	Turn OFF	1.5	6
07	Zn-MOF	MeCN	Turn OFF	0.73	7

Table S2: results of Hg(II) determination by the sensor **HL** in three real water samples

Water Sample	Added Hg(II) (μM)	Founded Hg(II) (μM)	Recovery (%)
Tap Water	0.0	0.18 ± 0.96	0.0
	2.0	1.93 ± 0.74	96.50
	5.0	4.98 ± 1.16	99.60
	10.0	10.48 ± 0.52	104.80
	20.0	19.62 ± 1.13	98.10
Distilled Water	0.0	0.08 ± 0.76	0.0
	2.0	1.88 ± 0.90	99.40
	5.0	4.82 ± 1.60	96.40
	10.0	10.54 ± 0.73	105.40
	20.0	20.57 ± 0.68	102.85
Industrial River water	0.0	0.26 ± 0.69	0.0
	2.0	1.97 ± 0.85	98.50
	5.0	5.12 ± 0.59	102.40
	10.0	10.64 ± 0.96	106.40
	20.0	20.88 ± 0.46	104.40

Table S3: results of Cd(II) determination by the sensor **HL** in three real water samples

Water Sample	Added Cd(II) (μM)	Founded Cd(II) (μM)	Recovery (%)
Tap Water	0.0	0.13 ± 0.69	0.0
	2.0	1.91 ± 0.85	95.50
	5.0	4.98 ± 1.01	99.60
	10.0	9.83 ± 0.89	101.75
	20.0	20.35 ± 0.73	98.10
Distilled Water	0.0	0.04 ± 0.91	0.0
	2.0	1.83 ± 0.90	91.50
	5.0	4.91 ± 0.75	98.20
	10.0	$10.44 \pm .51$	104.40
	20.0	19.87 ± 0.69	99.35
Industrial River water	0.0	0.26 ± 0.73	0.0
	2.0	1.87 ± 0.85	93.50
	5.0	5.26 ± 0.49	105.20
	10.0	10.84 ± 0.66	108.40
	20.0	19.88 ± 0.86	99.40

Referances

1. G. Chakraborty, S. K. Mandal, ACS Omega 2018, **3**, 3248-3256.
2. S. Gupta, M. D. Milton Journal of Photochem. & Photobiol A: Chem. 2021, **419** 113444.
3. S. Maity, M. Shyamal, D. Das, P. Mazumdar, G.P. Sahoo, A. Misra, *Sens. Actuators B Chem.*2017, **248**, 223–233.
4. S. Guo, J. Pan, J. Huang, L. Kong, J. Yang, Rsc Adv. 2019, **9**, 26043–26050.

5. S.S. Babu, S. Shanmugam, Metal-free γ , *Chemistry Select* 2018, **3**, 4075–4081.
6. S. Halder, P. Ghosh, A. Hazra, P. Banerjee and P. Roy, *New J. Chem.* 2018,**42**, 8408-8414.
7. Zhang, X.; Hu, J.; Wang, B.; Li, Z.; Xu, S.; Chen, Y.; Ma, X. *J. Solid State Chem.* 2019, **269**, 459-464.